Original Article

Single-cell transcriptomic, transcriptomic, and metabolomic characterization of human atherosclerosis

Xiaoyang Liu[1]^, Li Li[2], Yiru Yin[3], Likui Zhang[4], Wenhao Wang[5]^

[1]Department of Cardiology, Second Hospital of Shanxi Medical University, Taiyuan, China; [2]Department of Geriatrics, Second Hospital of Shanxi Medical University, Taiyuan, China; [3]Key Laboratory of Cellular Physiology, Ministry of Education, Department of Physiology, Shanxi Medical University, Taiyuan, China; [4]Department of Cardiovascular Surgery, Shanxi Bethune Hospital, Shanxi Academy of Medical Sciences, Taiyuan, China; [5]Department of Obstetrics and Gynecology, Second Hospital of Shanxi Medical University, Taiyuan, China

Contributions: (I) Conception and design: X Liu, W Wang; (II) Administrative support: X Liu, W Wang; (III) Provision of study materials or patients: L Li; (IV) Collection and assembly of data: Y Yin, L Zhang; (V) Data analysis and interpretation: X Liu, W Wang; (VI) Manuscript writing: All authors; (VII) Final approval of manuscript: All authors.

Correspondence to: Likui Zhang, MD. Department of Cardiovascular Surgery, Shanxi Bethune Hospital, Shanxi Academy of Medical Sciences, Taiyuan, China. Email: sxdyyxwkzlk@163.com; Wenhao Wang, MD. Department of Obstetrics and Gynecology, Second Hospital of Shanxi Medical University, Taiyuan, China. Email: wwh199459@sxmu.edu.cn.

Background: Atherosclerosis is the main cause of many cardiovascular and cerebrovascular diseases (CVDs), and gaining a deeper understanding of the intercellular connections and key central genes which mediate formation of atherosclerotic plaques is required.

Methods: We performed a comprehensive bioinformatics analysis of differential genetic screening, Kyoto Encyclopedia of Genes and Genomes (KEGG) signaling pathway annotation, protein-protein interactions (PPIs), pseudo-timing, intercellular communication, transcription factors on carotid single-cell sequencing data, and aortic bulk transcriptome and metabolomic data.

Results: Ten cell types were identified in the data: T cells, monocytes, smooth muscle cells, endothelial cells, B cells, fibroblasts, plasma cells, mast cells, dendritic cells, and natural killer cells. Endothelial, fibroblast, macrophage, and smooth muscle cell subtype differentiation trajectories, interaction networks, and important transcription factors were characterized in detail. Finally, using this information combined with transcriptome and metabolome analyses, we found the key genes and signaling pathways of atherosclerosis, especially the advanced glycation end products and receptor for advanced glycation end products signaling pathway (AGE-RAGE signaling pathway) in diabetic complications, linked the differential metabolites with fibroblasts and atherosclerosis and contributed to it in patients with diabetes.

Conclusions: Collectively, this study provides key genes, signaling pathways, cellular communication, and transcription factors among endothelial cells, fibroblasts, macrophages, and smooth muscle cells for the study of atherosclerotic plaques, and provides a basis for the diagnosis and treatment of atherosclerosis-like sclerosis.

Keywords: Atherosclerosis; single-cell analysis; gene expression profiling; genomics; metabolomics

---

^ ORCID: Xiaoyang Liu, 0000-0002-4062-1800; Wenhao Wang, 0000-0002-9216-5325.

Introduction

Cardiovascular and cerebrovascular diseases (CVDs) constitute the number one cause of death globally, including coronary heart disease, hypertension, and stroke (1,2). In 2019, the World Health Organization (WHO) reported more than 17.9 million people died of cardiovascular disease, accounting for 32% of global deaths, 85% of which were due to heart attack and stroke (3). Cardiovascular and other non-communicable diseases account for more than three-quarters of CVD deaths worldwide, often due to limited access to effective medical care and delays in CVD detection until late in the disease. This leads to an increase in cardiovascular and other non-communicable diseases, causing a disproportionate burden of disease in developing countries (4,5).

Carotid and coronary artery disease are the two major atherosclerotic diseases. Atherosclerotic disease in the coronary arteries can lead to myocardial ischemia and angina pectoris when the plaque stabilizes, and when the unstable plaque ruptures or erodes, thrombotic vascular occlusion and acute stroke or myocardial infarction (MI) may occur (6). Carotid atherosclerosis is a chronic disease of the carotid arteries caused by inflammation and the accumulation of lipid-rich plaques in the arterial walls. As the plaques expand, the blood vessels narrow, and blood flow to the brain decreases which may cause stroke (7). Carotid and coronary artery atherosclerosis have a poor prognosis and are interrelated and mutually causal. Plaques in both tend to occur at bifurcations and arterial bends (8), and both are often associated with multiple risk factors (9). Therefore, a combined analysis of carotid and coronary artery atherosclerosis could identify common factors in the development of the disease, which is of great significance for its diagnosis and treatment.

At the turn of this century, well-annotated tissue repositories and broader comprehensive molecular profiling techniques made it possible to understand the pathogenesis of atherosclerosis. The transcriptome is traditionally sequenced in mixed cell populations. Different cells are involved in atherosclerosis, with different genomes, which are difficult to decipher by traditional batch sequencing technology, and single-cell transcriptome sequencing (scRNA-seq) technology is more capable of resolving complex and diverse biological phenomena than traditional bulk genome sequencing methods (10).

In this study, we performed differential genetic screening, Kyoto Encyclopedia of Genes and Genomes (KEGG) signaling pathway annotation, protein-protein interactions (PPIs) analysis, and simulation of carotid atherosclerosis single-cell sequencing data, atherosclerotic transcriptome sequencing data (mRNA-seq), and metabolome sequencing data. Through a comprehensive bioinformatics analysis of timing, intercellular communication, and transcription factors, we identified 10 cell types, screened out important genes, signaling pathways, and metabolites in endothelial cells, fibroblasts, macrophages, and smooth muscle cells, and revealed cell-to-cell interaction networks and important transcription factors in the process of development of atherosclerosis. We present the following article in accordance with the MDAR reporting checklist (available at https://atm.amegroups.com/article/view/10.21037/atm-22-4852/rc).

Methods

Patient sample collection

This study was conducted in accordance with the Declaration of Helsinki (as revised in 2013) and was approved by the Medical Ethics Committee of the Second Hospital of Shanxi Medical University (No. 2021YX138). Written informed consent was obtained from all subjects. Vessel wall specimens were collected from patients who had undergone aortic dissection as part of aortic replacement surgery. The control group included patients who had undergone aortic dissection without aortic plaque, and the experimental group included patients who had undergone aortic dissection with aortic plaque. Transcriptome sequencing and untargeted metabolomic sequencing used three aortic dissection samples without aortic plaques, and three aortic dissection samples with aortic plaques.

Additionally, this study used an Illumina NextSeq 500-based single-cell sequencing dataset (scRNA-seq) (GSE159677, https://www.ncbi.nlm.nih.gov) of human carotid endarterectomy tissue with a 10× genomics read depth. The analysis included three carotid atherosclerotic cores and three proximal adjacent tissues, with a total of 51,981 cells sequenced.

RNA preparation, cDNA library preparation, and sequencing

Sample RNA was isolated and purified using TRIzol (cat. 15596018; Thermo Fisher Scientific, Waltham, MA, USA) according to the manufacturer's instructions. The quantity and purity of total RNA were then quality controlled using the NanoDrop ND-1000 (NanoDrop Technologies, Wilmington, DE, USA) and the integrity of RNA was

checked using a Bioanalyzer 2100 (Agilent Technologies Co. Ltd., Palo Alto, CA, USA). Concentrations >50 ng/µL, RIN value >7.0, and total RNA >1 µg were sufficient for downstream experiments. The RNA was subsequently reverse transcribed to cDNA using SuperScript™ II reverse transcriptase (Invitrogen, cat. 1896649, USA). cDNA was purified using E. coli DNA polymerase I (NEB, cat. m0209, USA), RNaseH (NEB, cat. m0297, USA), and dUTP solution (Thermo Fisher, cat. R0133, USA). Following this, the junction was ligated to the A-tailed fragment DNA and further purification was performed. Finally, amplification was conducted by PCR, and 2×150 bp double-end sequencing (PE150) was performed using Illumina Novaseq™ 6000 (LC-Bio Technology Co., Ltd., Hangzhou, China). The amplification conditions were as follows: Initial denaturation at 95 ℃ for 3 min; denaturation at 98 ℃ for 15 s, annealing at 60 ℃ for 15 s, extension at 72 ℃ for 30 s for eight cycles; and final extension at 72 ℃ for 5 min.

Metabolite extraction

A 50% methanol buffer was used to extract metabolites from samples after they were thawed on ice. We extracted 20 µL of sample with 120 µL of precooled 50% methanol, vortexed for 1 min, and incubated at room temperature for 10 min; the extraction mixture was then stored overnight at –20 ℃. As soon as the supernatants were centrifuged for 20 minutes at 4,000 g, they were transferred to 96-well plates. Prior to LC-MS analysis, samples were stored at –80 ℃. Additionally, pooled QC samples were prepared by combining 10 µL of each extraction mixture (11).

Triple quadrupole LC-MS parameter settings

All metabolite samples were collected using an LC-MS system according to the instructions of the product specification. Chromatographic separation was first performed using a Thermo Scientific UltiMate 3000 and reversed-phase separation was performed on an ACQUITY UPLC BEH C18 column (100 mm × 2.1 mm, 1.8 µm, cat. 186002350; Waters Ltd., Wilmslow, England). Finally, the metabolites eluted from the column were detected using a high-resolution tandem mass spectrometer TripleTOF6600plus (SCIEX, Framingham, MA, USA).

mRNA differentially expressed gene (DEG) analysis

The edgeR (12) algorithm was applied to filter the mRNA-

seq data set, and the differentially expressed mRNAs were screened, with the difference fold $|log2(FC)| \geq 1$ and q value <0.05 as the standard, it was considered as the screening conditions. The screened genes are considered as differentially expressed genes.

Untargeted metabolomic analysis

MS data were pre-processed using XCMS software (version ="3.8"), followed by conversion of LC-MS raw data to mzXML format, then further processing using XCMS, CAMERA and the metaX R package (13). Metabolites were identified and validated against a library of KEGG, HMDB, and internal metabolite fragment profiles by combining retention time and m/z data to identify each ion. Finally, the peak data were further processed using metaX. Missing values were processed using k-NearestNeighbor, and principal component analysis was performed for outliers.

ScRNA-seq data processing

ScRNA-seq QC
The initial gene expression matrix was processed and analyzed using the Seurat software package (version 4.1.0) (14). The conditions were set such that the number of genes in the cells was greater than 500, the RNA counts per cell were greater than 4,000, and the percentage of mitochondrial reads was less than 20%.

Dimensionality reduction, clustering, and visualization
After filtering, the expression matrix was normalized using the NormalizeData function in the Seurat package and ln transformed [ln (CPM+1)]. Principal component analysis was then applied using "RunPCA" with highly variable genes as input. Clustering was performed using a graph-based clustering algorithm and visualized using the Seurat function "Run tSNE." To address batch effects across datasets, we performed data integration using canonical correlation analysis in the Seurat package (15). For this analysis, the parameters of the study settings involved "SelectIntegrationFeatures" and "FindCluster" selecting the 2,000 genes with the greatest variation, along with the top 20 correlation vectors.

SCENIC analysis
We attempted to characterize regulators of transcription in different subpopulations of cells using the R package SCENIC (version 1.2.2) (16). |logFC| >0.5 and P value <0.05, were considered statistically significant.

Pseudo-time analysis

Based on the results of the Seurat analysis, we used monocle2 (17) for cell trajectory inference analysis. This package is frequently used in development-related research and can infer the differentiation trajectory of cells during the development or evolution of cell subtypes. To analyze the differentiation of carotid atherosclerotic plaques and proximal adjacent tissue cell trajectories and key genetic changes, we studied the expression patterns of key genes, ordered individual cells in pseudo-time, and simulated the dynamic changes of cells during development in pseudo-time.

Intercellular communication

Communication between cell clusters via ligands and receptors was analyzed using CellChat (18). Cell-cell networks in a total of eight cell clusters were explored and the differences in signaling pathways between the no plaque and plaque-formed groups were compared. Statistical significance was set at P<0.05.

Analysis of DEGs

Seurat FindMarkers was used to explore DEGs between different cell subsets and calculate the differential genes. Screening conditions were P<0.05, |log2(FC)| ≥1, and the results were used subsequently annotated using the GO and KEGG databases.

KEGG annotations

Enrichment analysis was based on the principle of hypergeometric distribution, and clusterProfiler software (19) was used to perform GO function and KEGG enrichment analysis on DEGs with high and low expression in different cell types. Statistical significance was set at P<0.05.

Analysis of PPI

The STRING database (https://string-db.org/) (20) was used to predict the PPI network in atherosclerosis. The minimum required interaction score for the network was 0.4, to analyze the functional interactions between proteins and help clarify the mechanism of occurrence and development of atherosclerosis. The PPI network was constructed using the STRING database, and the Cytoscape plugin cytohubba screened for hub genes in the network (21).

Statistical analysis

Student's *t*-tests were conducted to detect differences in metabolite concentrations between the two phenotypes, and the P value was adjusted for multiple tests using the false discovery-rate controlling Benjamini-Hochberg procedure. R (version 4.1.3) software was used to perform statistical analysis, and a P value <0.05 denoted statistical significance.

Results

Atherosclerosis mRNA-seq differential gene screening

Transcriptome sequencing of three aortic dissection samples with and three without aortic plaque was performed (*Figure 1*), and the results showed 1,099 genes were differentially expressed between the two groups, of which 574 were expressed in both. Five hundred and seventy-four genes were more highly expressed in those with arterial plaques than those without aortic plaques, and 525 genes were expressed less in samples with aortic plaques than in those without aortic plaques (*Figure 2A,2B*). KEGG annotation of the 574 upregulated genes revealed they were associated with the PPAR signaling pathway, cytokine-cytokine receptor interactions, osteoclast differentiation, African trypanosomiasis, aldosterone synthesis and secretion, carbohydrate digestion and absorption, cortisol synthesis and secretion, malaria, calcium signaling pathways, the MAPK signaling pathway, and others (*Figure 2C*). KEGG annotation of the 525 downregulated genes revealed they were associated with the cell cycle, oocyte meiosis, the p53 signaling pathway, progesterone-mediated oocyte maturation, human T-cell leukemia virus 1 infection, the Fanconi anemia pathway, homologous recombination, cellular senescence, asthma, cell adhesion molecules, and others (*Figure 2D*).

Screening of differential metabolites in atherosclerosis

LC-MS was used to detect the metabolite molecules between samples with and without aortic plaque and revealed 247 significantly different metabolite molecules. One hundred and thirty-eight molecules were more highly expressed in the aortic plaque group than in the non-aortic plaque group, and 109 metabolite molecules were less expressed in the aortic plaque group than in the non-aortic plaque group (*Figure 3A,3B*). KEGG annotation showed the top 10 signaling pathways were caffeine metabolism,
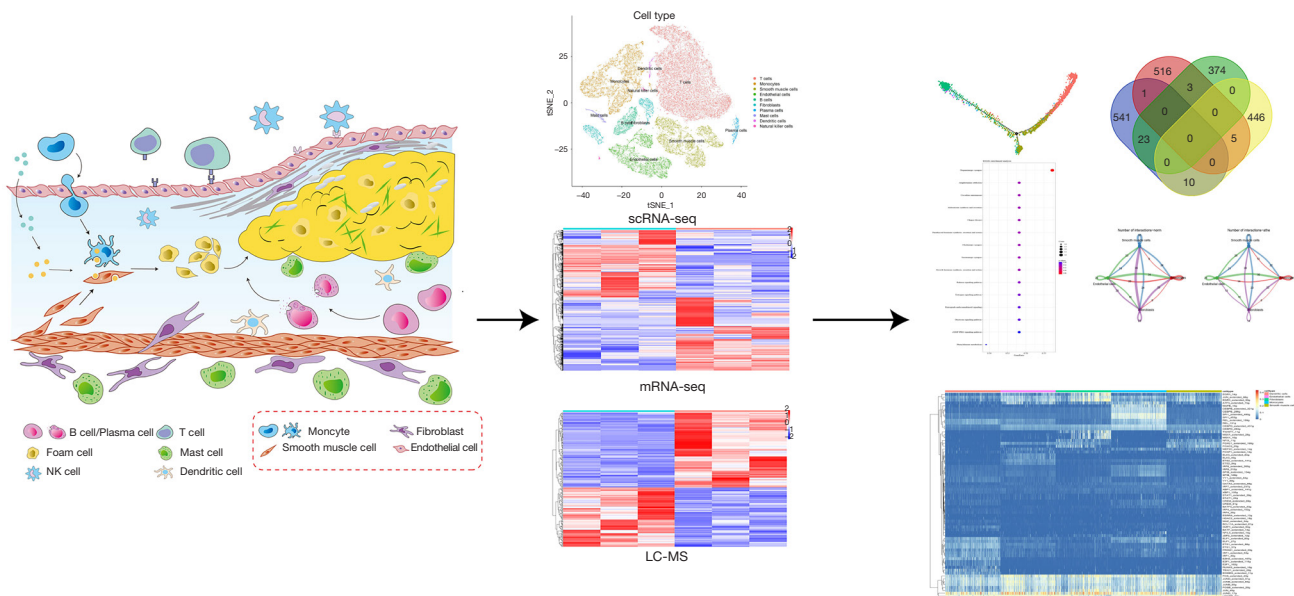
Figure 1 Overview of integrated bioinformatics analysis of the scRNA-seq, mRNA-seq, and LC-MS from patients with atherosclerosis. A total of 40,049 cells were clustered into 10 different cell types, including T cells, monocytes, smooth muscle cells, endothelial cells, B cells, fibroblasts, plasma cells, mast cells, dendritic cells, and natural killer cells. Combined bulk transcriptome and metabolome analysis was performed for key gene screening, signaling pathway annotation, cellular communication, and transcription factor analysis in endothelial cells, fibroblasts, macrophages, and smooth muscle cells. NK, natural killer cell; LC-MS, liquid chromatography-mass spectrometry.

neutrophil extracellular trap formation, vitamin digestion and absorption, the insulin signaling pathway, non-alcoholic fatty liver disease, the AGE-RAGE signaling pathway in diabetic complications, glucagon signaling pathways, insulin secretion, type II diabetes mellitus, and nitrogen metabolism, and the related metabolic small molecules were xanthine, N-acetyl-methionine leucine phenylalanine, hexamethylene diisocyanate, glucose, theobromine, vitamin K, and Malt tetraose sugar (*Figure 3C*).

scRNA-seq and cell types in atherosclerosis

Our scRNA-seq data were derived from GSE159677, including three cases of carotid atherosclerotic plaques and three cases of proximal adjacent tissue of the carotid artery tissue (*Figure 4A*). Three patients with atherosclerosis underwent scRNA-seq sequencing followed by quality filtering, yielding a total of 40,049 cells and an average of 1,651.28 genes. Based on the top five cell surface marker genes, we divided the cells into 10 cell types (*Figure 4B,4C*): T cells (*CCL5*, cluster 0), monocytes (*SPP1*, cluster 1), smooth muscle cells (*TAGLN*, cluster 1 and 2), endothelial cells (*ACKR1*, cluster 3 and 5), B cells (*MS4A1*, cluster 4),

fibroblasts (*FRZB*, cluster 6 and 7), plasma cells (*IGLC3*, cluster 8), mast cells (*TPSAB1*, cluster 7 and 9), dendritic cells (*CENPF*, cluster 10), and natural killer cells (*IRF7*, cluster 11) (*Figure 4D*).

### Endothelial cell populations in atherosclerotic plaques

Endothelial cell damage plays an important role in the development of atherosclerosis. We performed t-SNE subgrouping of endothelial cells and divided them into five clusters using hypervariable genes: *HLA-DPA1*, *COL4A1*, *ITLN1*, *SOST*, and *CCL5* endothelial cells (*Figure 5A,5B*). DEGs in the plaque group and proximal normal tissue in scRNA-seq were then compared with those in the plaque and no plaque groups in mRNA-seq. *TIMP3*, *MAOA*, *TSPAN7*, *TSHZ2*, *PREX2*, *CCL14*, *CAVIN2*, *LFNG*, *PDE2A*, *NRN1*, *MGLL*, *PLCB4*, *SPRY1*, *CYTL1*, *FOS*, *APOLD1*, *SPARCL1*, *ITM2A*, *CCDC69*, *LRG1*, *DOC2B*, *TNFSF9*, and *CFD* were highly expressed in the plaque group, and *IGFBP5*, *IGKC*, *NRGN*, *IGHA1*, and *CRTAC1* were less expressed in the plaque group (*Figure 5C*). Pseudo-chronological analysis showed endothelial cells in the non-plaque group were mostly *HLA-DPA1* endothelial
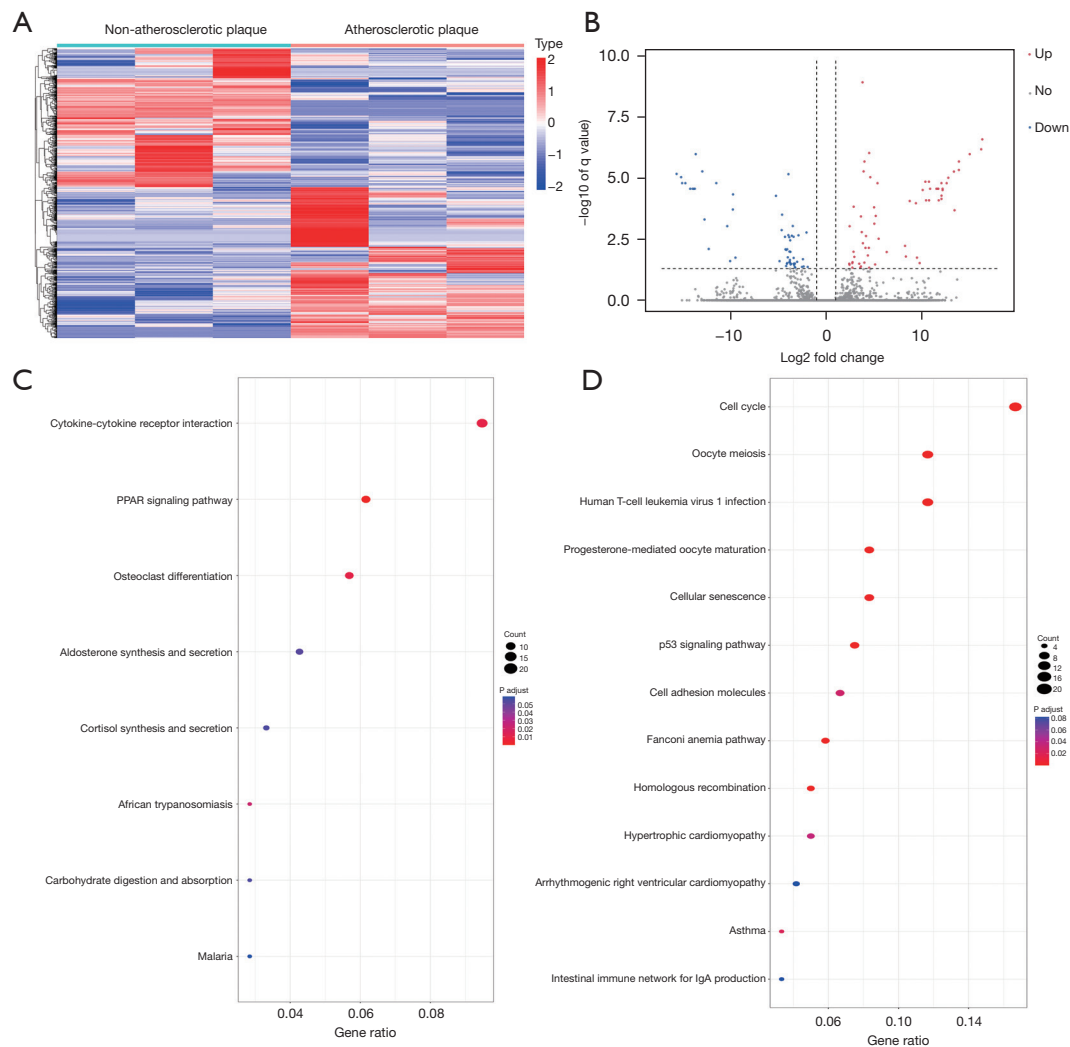
Figure 2 Differential gene analysis between atherosclerotic and non-atherosclerotic plaque groups. (A) Heatmap of differential gene expression. A gradual change in color from blue to red indicates downregulated to upregulated gene expression. (B) Volcano plot of differential gene expression, with red nodes representing up-regulation and blue nodes representing down-regulation. (C) KEGG signaling pathway enrichment of upregulated genes. Y-axis labels represent clustered KEGG pathways, and gene ratio represents the ratio of the number of enriched genes to the number of upregulated differential genes in the KEGG pathway. (D) KEGG signaling pathway enrichment of downregulated genes. Y-axis labels represent clustered KEGG pathways. Gene ratio represents the ratio of the number of enriched genes to the number of downregulated differential genes in the KEGG pathway. KEGG, Kyoto Encyclopedia of Genes and Genomes.

cells with some *COL4A1* endothelial cells, whereas those in the plaque group were *ITLN1*, *CCL5*, and *SOST* endothelial cells, with some *COL4A1* endothelial cells (*Figure 5D,5E*). The 28 intersecting gene-related signaling pathways were related to dopaminergic synapses, amphetamine addiction, circadian entrainment, aldosterone synthesis and secretion, Chagas disease, parathyroid hormone synthesis, secretion

and action, cholinergic synapse, serotonergic synapse, growth hormone synthesis, secretion and action, the relaxin signaling pathway, the estrogen signaling pathway, retrograde endocannabinoid signaling, the oxytocin signaling pathway, the cGMP-PKG signaling pathway, phenylalanine metabolism, the chemokine signaling pathway, histidine metabolism, tyrosine metabolism, and
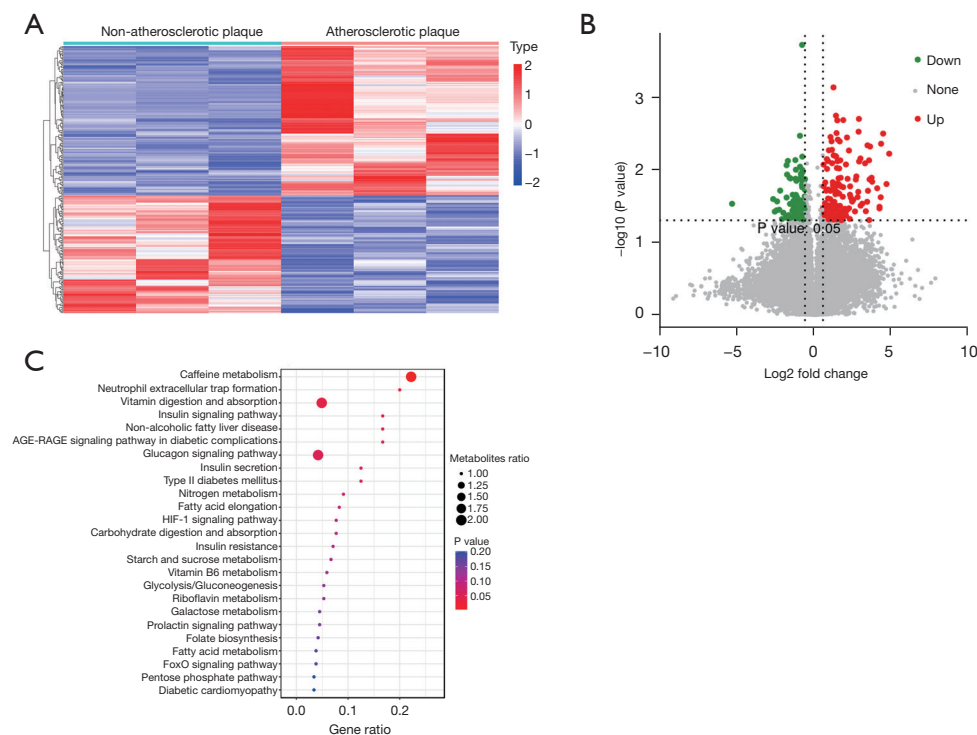
Figure 3 Analysis of differential metabolites between atherosclerotic and non-atherosclerotic plaque groups. (A) Heat map of differential metabolite expression. A gradual change in color from blue to red indicating downregulated to upregulated metabolite expression. (B) Volcano plot of differential metabolite expression, with red nodes representing up-regulation and green nodes representing down-regulation. (C) Differential metabolite KEGG signaling pathway enrichment, with y-axis labels representing aggregated KEGG pathways. Metabolites Ratio represents the ratio of the number of enriched metabolites to the number of differential genes in the KEGG pathway. KEGG, Kyoto Encyclopedia of Genes and Genomes.

African trypanosomiasis (*Figure 5F*).

Fibroblast populations in atherosclerotic plaques

This study used t-SNE to subgroup fibroblasts into four clusters: *RGS5*, *APOD*, *SFRP5*, and *GZMA* fibroblasts (*Figure 6A,6B*). Fifty-six genes were highly expressed in both scRNA-seq and mRNA-seq of samples with plaques: *RDH10*, *GFPT2*, *MAOA*, *TSPAN7*, *CNTFR*, *MFAP5*, *MGST1*, *VIT*, *SVEP1*, *FKBP5*, *PALM*, *ANGPTL4*, *NTRK2*, *SPRY1*, *NR4A1*, *APOD*, *WNT11*, *MYOC*, *THBS1*, *CCDC69*, *LRRN4CL*, *FOSB*, *MT1A*, *CFD*, *CXCL14*, *CHRDL1*, *ITIH5*, *TIMP3*, *PLA2G2A*, *TSHZ2*, *EMP1*, *CD248*, *SLPI*, *FLNB*, *AGTR1*, *ADGRD1*, *MGLL*, *SCARA5*, *PRG4*, *PTGDS*, *IGSF10*, *FOS*, *GLUL*, *SPARCL1*, *RASD1*, *ANPEP*, *ITM2A*, *OAF*, *GPX3*, *SIX1*, *GPRC5B*, *HSD11B1*, *PI16*, *F3*, *SFRP1*, and *RETREG1* (*Figure 6C*). Ten genes

were under-expressed in both scRNA-seq and mRNA-seq of samples with plaques: *ACTC1*, *STMN1*, *IGKC*, *SAMD11*, *NRGN*, *MT1F*, *SOD3*, *SGCG*, *VCAM1*, and *CRTAC1* (*Figure 6C*). Pseudo-chronological analysis revealed APOD fibroblasts gradually differentiated into *SFRP5*, *RGS5*, and *GZMA* fibroblasts as blood vessels transitioned from a state of no plaques to plaques (*Figure 6D,6E*). The 66 genes with the same expression trend in scRNA-seq and mRNA-seq were enriched in signaling pathways including glutathione metabolism, arachidonic acid, amphetamine addiction, renin-angiotensin system, Cushing syndrome, MAPK signaling pathway, the AGE-RAGE signaling pathway in diabetes complications, alanine, aspartate, and glutamate metabolism, proteoglycans in cancer, cocaine addiction, malaria, fluid shear stress and atherosclerosis, mineral absorption, cortisol synthesis and secretion, drug metabolism (cytochrome P450), and metabolism of
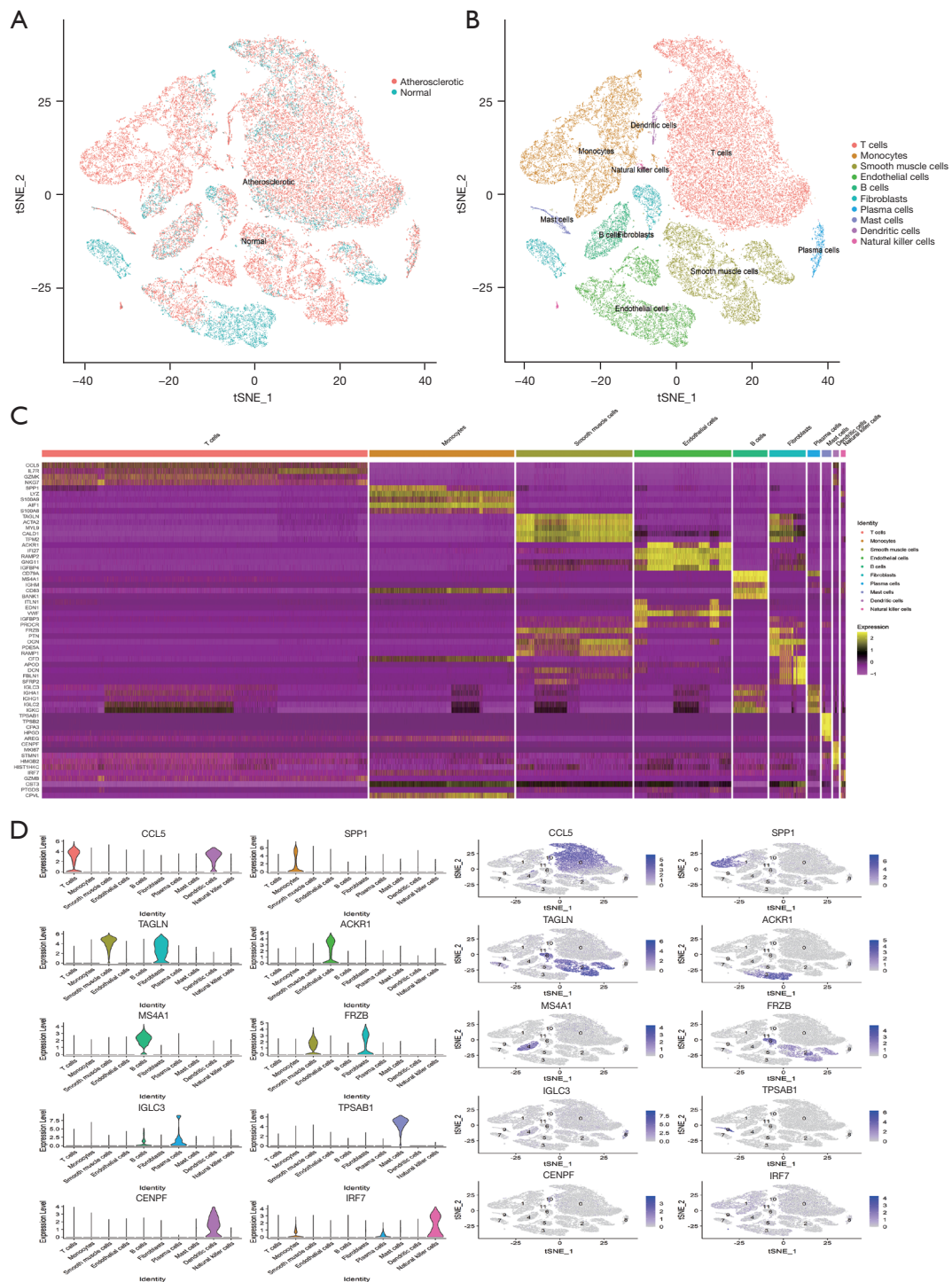
Figure 4 Identification of atherosclerotic cell populations. (A) t-SNE showing atherosclerotic plaque and proximal adjacent tissue populations of arterial tissue. (B) t-SNE displays atherosclerotic cell types. (C) Heatmap showing the top five expressed genes per cell cluster. (D) Representative marker genes of atherosclerotic cell types, with relative expression levels from low to high indicated by colors ranging from gray to blue. Gene expression levels were normalized using LogNormalize in Seurat. t-SNE, t-distributed stochastic neighbor embedding.
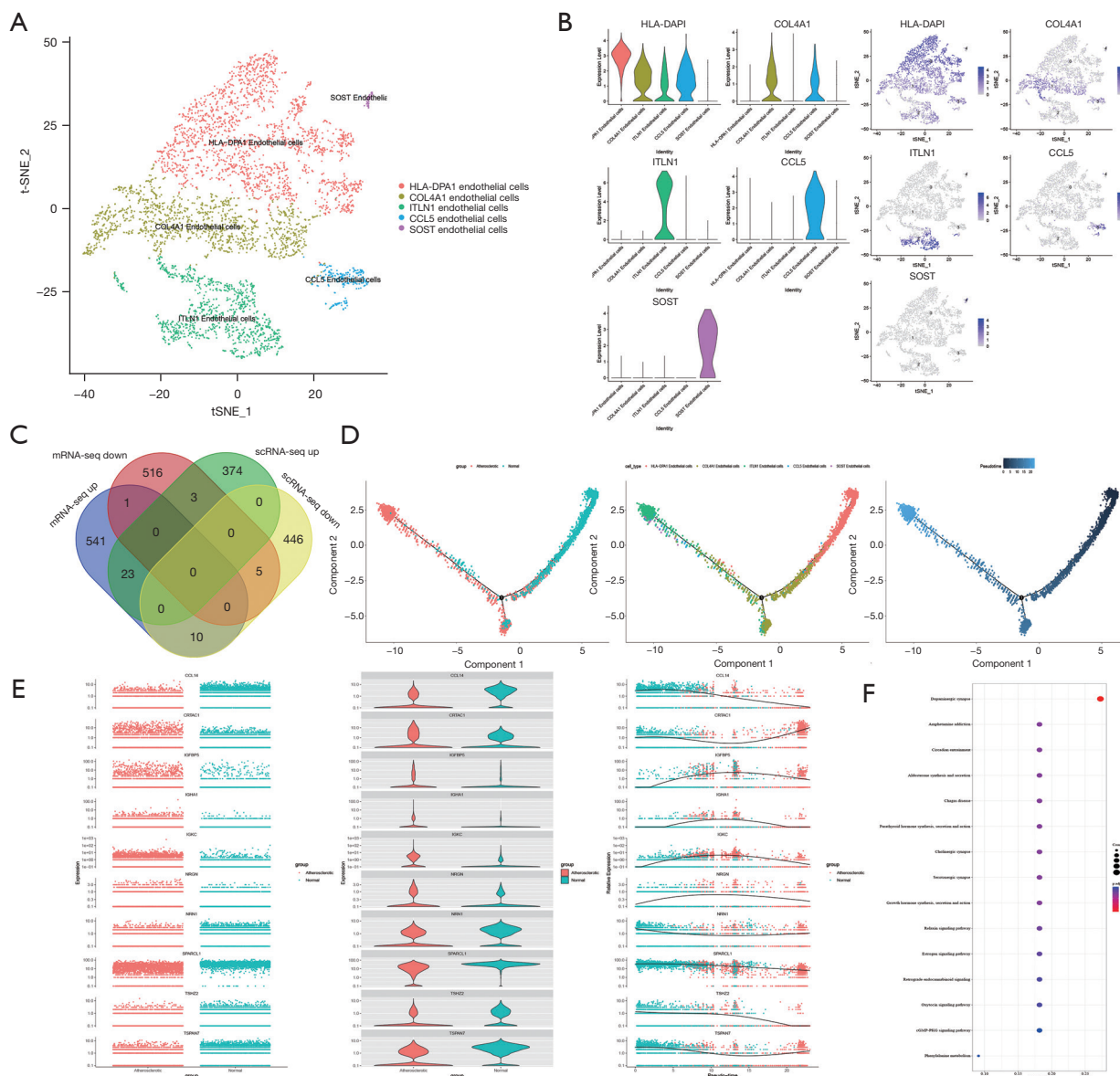
Figure 5 Atherosclerotic endothelial cell repopulation and expression patterns. (A) t-SNE demonstrates atherosclerotic endothelial subset cell types. (B) Violin plot showing representative marker genes for endothelial cell subsets, with relative expression levels from low to high indicated by colors ranging from gray to blue. (C) The intersection of scRNA-seq and mRNA-seq differential genes in the atherosclerotic plaque group compared with the non-atherosclerotic plaque group. (D) Pseudo-chronological analysis trajectories of endothelial cells inferred by Monocle2, with each point corresponding to a cell. (E) Pseudo-chronological analysis trajectory of the top 10 differential genes of endothelial cells in the atherosclerotic plaque group compared with the non-atherosclerotic plaque group. (F) Bubble plot showing enrichment of the KEGG signaling pathway for genes at the intersection of scRNA-seq and mRNA-seq. t-SNE, t-distributed stochastic neighbor embedding; KEGG, Kyoto Encyclopedia of Genes and Genomes.
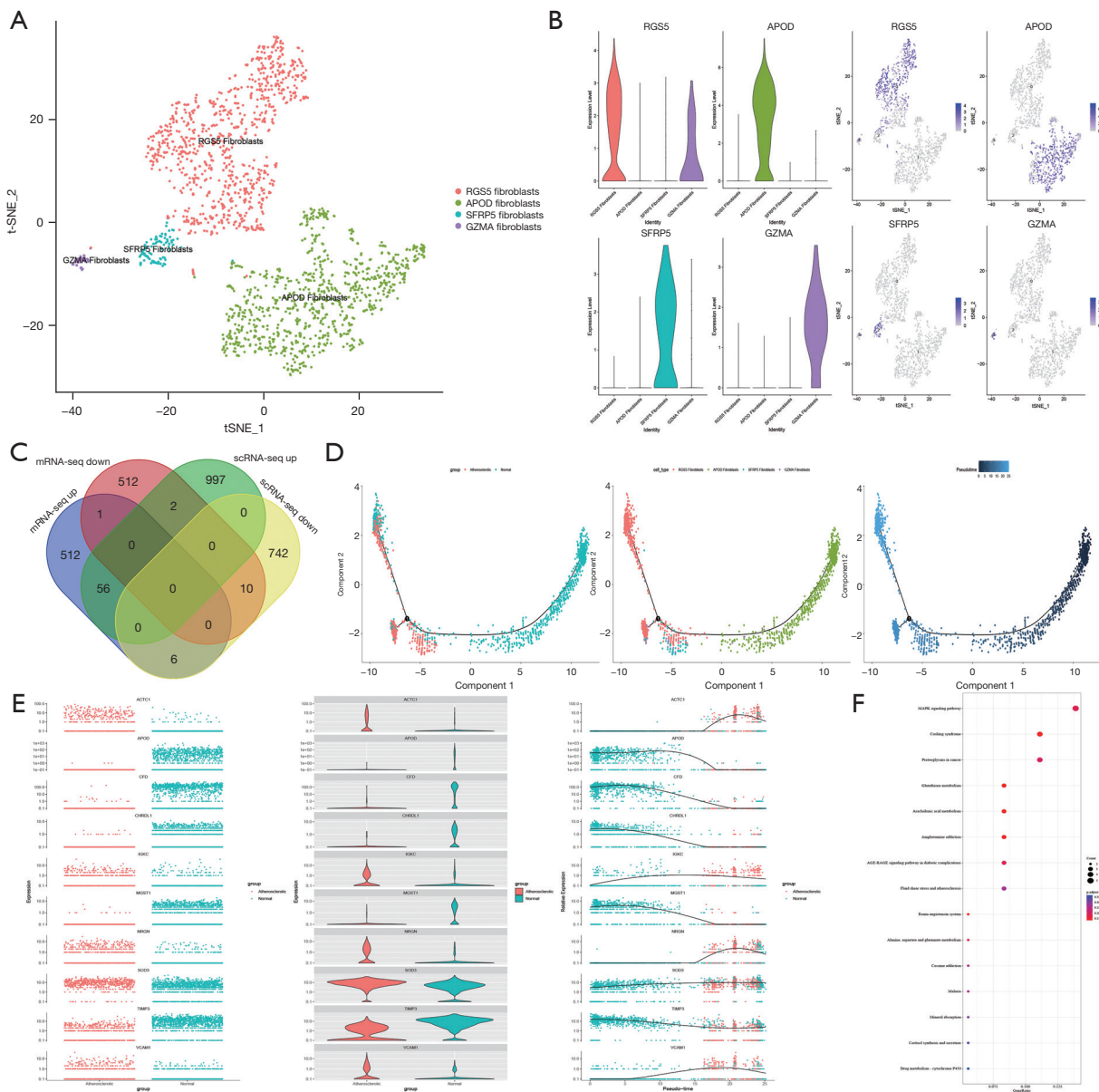
Figure 6 Atherosclerotic fibroblast repopulation and expression patterns. (A) t-SNE demonstrates atherosclerotic fibroblast cell types. (B) Violin plot showing representative marker genes for fibroblast subpopulations, with relative expression levels from low to high indicated by colors ranging from gray to blue. (C) The intersection of scRNA-seq and mRNA-seq differential genes in the atherosclerotic plaque group compared with the non-atherosclerotic plaque group. (D) Pseudo-chronological analysis trajectories of fibroblasts inferred by Monocle2, with each point corresponding to a cell. (E) Pseudo-chronological analysis trajectory of the top 10 differential genes of fibroblasts in the atherosclerotic plaque group compared with the non-atherosclerotic plaque group. (F) Bubble plot showing enrichment of the KEGG signaling pathway for genes at the intersection of scRNA-seq and mRNA-seq. t-SNE, t-distributed stochastic neighbor embedding; KEGG, Kyoto Encyclopedia of Genes and Genomes.

xenobiotics by cytochrome P450 (*Figure 6F*).

Macrophage phenotype in atherosclerotic plaques

The monocyte cell population was divided into *C1QB*, *FABP4*, *APOBEC3A*, *IL7R*, *CCL13*, and *CALD1* monocytes using the hypervariable genes (*Figure 7A,7B*). Both scRNA-seq and mRNA-seq showed *LILRB2*, *FGR*, *KCNE1*, *CSF3R*, *CLEC4E*, *FCN1*, *EMP1*, *EGR2*, *DUSP1*, *APOBEC3A*, *NCF1*, *FKBP5*, *PTX3*, *S100A8*, *LILRA5*, *TMEM154*, *PADI4*, *IL1R2*, *NR4A1*, *FOS*, *THBS1*, *ACSL1*, *LILRA1*, *CLEC12A*, *CCDC69*, *LRG1*, *FPR2*, *FOSB*, *CFP*, *S100A12*, *VNN2*, *CFD*, *CH25H*, *FOLR3*, *VSTM1*, and *S100A9* were highly expressed in the plaque group compared with the proximal normal tissue. Expression of *ADAMDEC1*, *ARL4C*, *CD72*, *IGKC*, *CYP27A1*, and *MT1F* were lower in the plaque group than in the proximal normal tissue (*Figure 7C*), which contained mostly *CCL13* and *APOBEC3A* monocytes. When plaques occurred, most monocytes were transformed into *C1QB*, *FABP4*, *IL7R*, and *CALD1* monocytes (*Figure 7D,7E*). The KEGG signaling pathways enriched for genes upregulated or downregulated in the plaque group in scRNA-seq and mRNA-seq were osteoclast differentiation, the B cell receptor signaling pathway, the *IL-17* signaling pathway, fluid shear stress and atherosclerosis, primary bile acid biosynthesis, amphetamine addiction, the PPAR signaling pathway, leishmaniasis, human T-cell leukemia virus 1 infection, Staphylococcus aureus infection, and hematopoietic cell lineage (*Figure 7F*).

Smooth muscle cells in atherosclerotic plaques

We further classified BCAM smooth muscle cells into *TFPI2*, *SFRP2*, *ACTC1*, and *CXCR4* smooth muscle cells (*Figure 8A,8B*). Pseudo-chronological analysis showed the normal arterial tissues were mostly BCAM smooth muscle cells, and when atherosclerosis occurred, smooth muscle cells were mostly from the TFPI2 and SFRP2 subtypes. The co-upregulated genes by scRNA-seq and mRNA-seq were *ITIH5*, *TIMP3*, *DES*, *FHL5*, *MGLL*, *ANGPTL4*, *NTRK2*, *NR4A1*, *FOS*, *APOLD1*, *THBS1*, *RASD1*, *FABP4*, *FOSB*, *MT1A*, *CASQ2*, and *CFD*, while the downregulated genes were *ARL4C*, *GAP43*, *STMN1*, *PDGFRL*, *FAP*, *IGKC*, *IGHA1*, *CRTAC1*, and *TFPI2* (*Figure 8C*). ACTC1 and CXCR4 smooth muscle cells were present in both normal arterial and atherosclerotic tissues (*Figure 8D,8E*). The enriched signaling pathways of these 35 genes were the MAPK signaling pathway, regulation
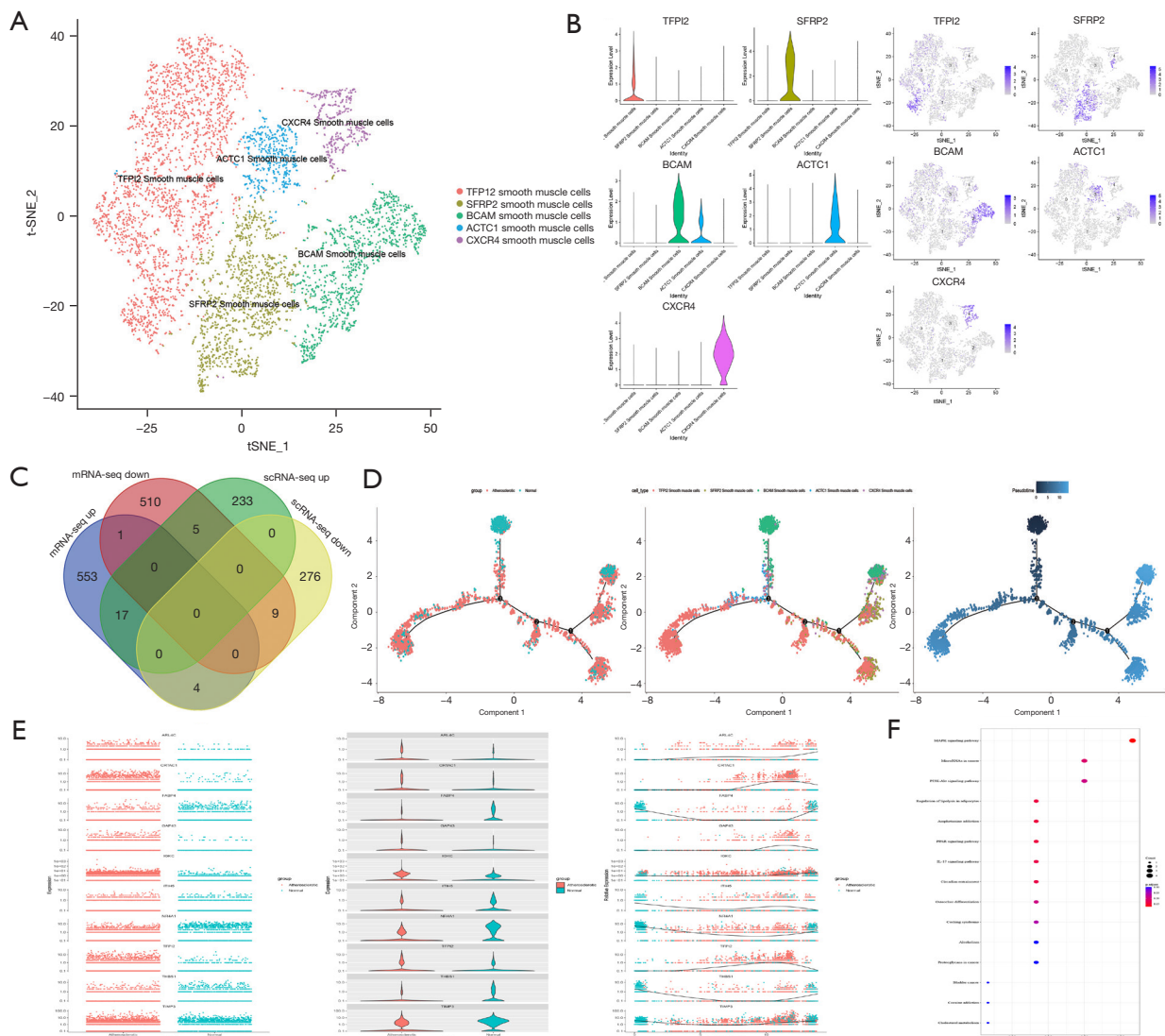
of lipolysis in adipocytes, amphetamine addiction, the PPAR signaling pathway, the IL-17 signaling pathway, circadian entrainment, microRNAs in cancer, osteoclast differentiation, the PI3K-Akt signaling pathway, Cushing syndrome, and alcoholism (*Figure 8F*).

Inference of cell-to-cell communication

PPI analysis was performed on the co-up and co-downregulated genes using scRNA-seq and mRNA-seq, and showed *FGR*, *S100A9*, *LILRB2*, *S100A12*, *S100A8*, *FCN1*, *S100A9*, *CSF3R*, *LILRA1*, and *VNN2* as the top 10 proteins in the PPI network (*Figure 9A*). These hub proteins were also associated with macrophages. CellChat was used to further explore the interactions between endothelial cells, fibroblasts, monocytes, and smooth muscle cells, and overall, the number and strength of cell-to-cell interactions were attenuated as blood vessels developed atherosclerosis (*Figure 9B*). Analysis of conserved and specific signaling pathways revealed *MPZ*, *HGF*, *IGF*, *IL6*, *CSF*, *SELPLG*, *OSM*, *ANGPTL*, *SEMA3*, *SELL*, *RESISTIN*, *GRN*, *FGF*, *SELE*, *TENASCIN*, and *COMPLEMENT* were expressed in proximal normal tissues only, whereas SPP1 was expressed in the plaque group only (*Figure 9C*). Overall, the number and strength of cell-to-cell interactions were attenuated during plaque development, whereas both macrophages and smooth muscle cells were increased in the plaque group. The *CD99*, *APP*, *CCL*, *MK*, *CXCL*, *LAMININ*, *PECAM1*, *VEGF*, and *SPP1* signaling pathways were increased in macrophages in the plaque group, while the increased signaling pathways in smooth muscle cells in the plaque group were *CD99*, *APP*, *JAM*, *PROS*, *PERIOSTIN*, *VCAM*, and *SPP1* (*Figure 9D*). Endothelial cells and fibroblasts were mostly attenuated in the plaque group, and only *PTN*, *MHC-I*, and *VCAM* were enhanced in the fibroblast plaque group (*Figure 9D*).

We then set endothelial cells and smooth muscle cells as senders and macrophages and fibroblasts as receivers to facilitate the interpretation of the effects of endothelial cells and smooth muscle cells on macrophages and fibroblasts in atherosclerosis. Ligand-receptor contrast analysis was performed using bubble plots to show up- or downregulated ligand-receptor pairs. The highly expressed ligand-receptor pairs in atherosclerotic tissues with endothelial cells as senders and macrophages as receivers were *APP-CD74*, *CD99-PILRA*, *COL4A1-CD44*, *COL4A2-CD44*, *CXCL12-CXCR4*, *FN1-(ITGA4 + ITGB1)*, *LAMA4-CD44*, *LAMB1-CD44*, *LGALS9-CD44*, *LGALS9-CD45*, *LGALS9-*

Figure 7 Atherosclerotic macrophage repopulation and expression patterns. (A) t-SNE demonstrates atherosclerotic macrophage cell types. (B) Violin plot showing representative marker genes for macrophage subsets, with relative expression levels from low to high indicated by colors ranging from gray to blue. (C) The intersection of scRNA-seq and mRNA-seq differential genes in the atherosclerotic plaque group compared with the non-atherosclerotic plaque group. (D) Pseudo-chronological analysis trajectories of macrophages inferred by Monocle 2, with each dot corresponding to a cell. (E) Pseudo-chronological analysis trajectory of the top 10 differential genes of macrophages in the atherosclerotic plaque group compared with the non-atherosclerotic plaque group. (F) Bubble plot showing enrichment of KEGG signaling pathway for genes at the intersection of scRNA-seq and mRNA-seq. t-SNE, t-distributed stochastic neighbor embedding; KEGG, Kyoto Encyclopedia of Genes and Genomes.
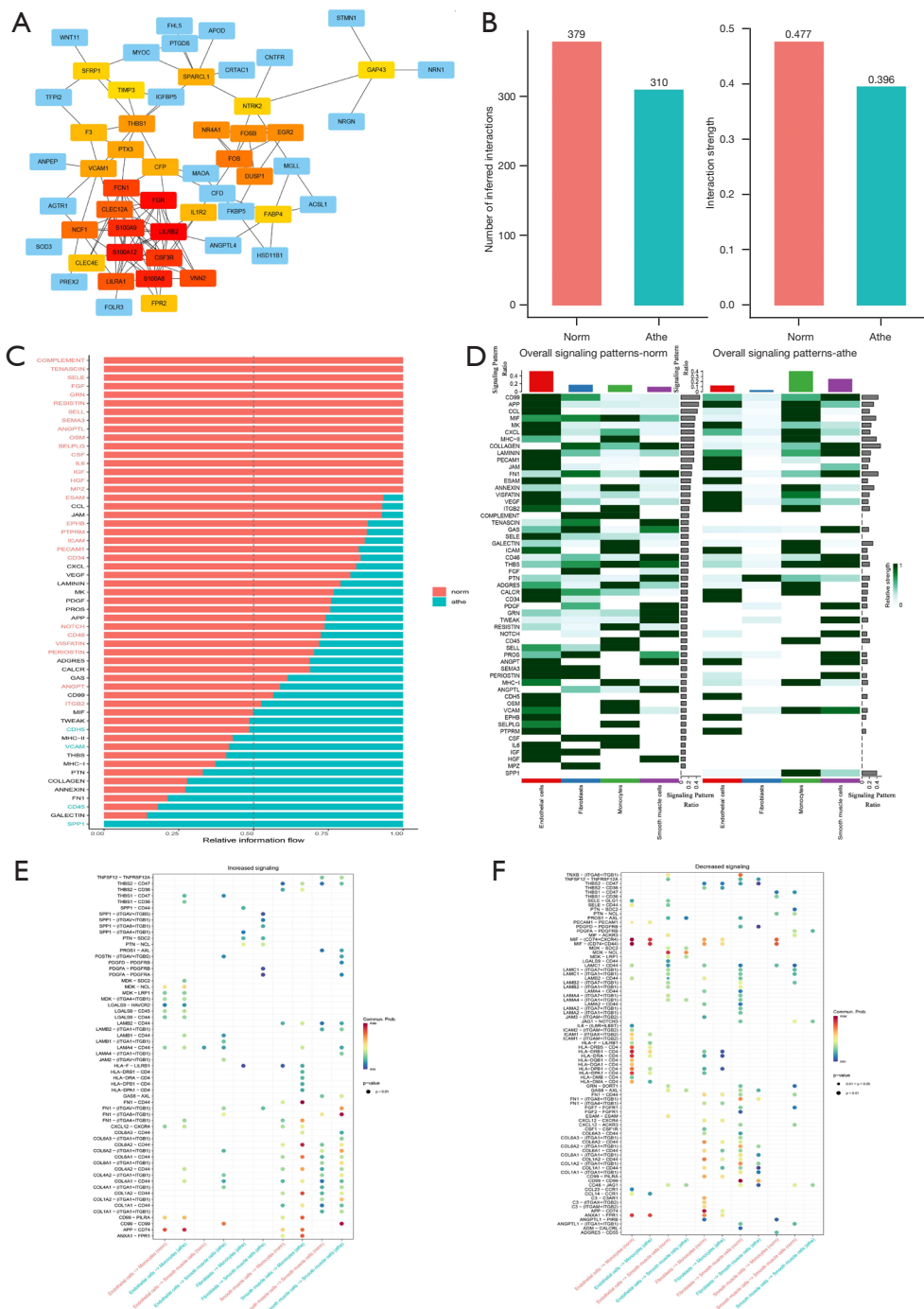
Figure 8 Atherosclerotic smooth muscle cell repopulation and expression patterns. (A) t-SNE demonstrates atherosclerotic smooth muscle cell types. (B) Violin plot showing representative marker genes for smooth muscle cell subsets, with relative expression levels from low to high indicated by colors ranging from gray to blue. (C) The intersection of scRNA-seq and mRNA-seq differential genes in the atherosclerotic plaque group compared with the non-atherosclerotic plaque group. (D) Pseudo-chronological analysis trajectories of smooth muscle cells inferred by Monocle2, with each point corresponding to a cell. (E) Pseudo-chronological analysis trajectory of the top 10 differential genes of smooth muscle cells in the atherosclerotic plaque group compared with the non-atherosclerotic plaque group. (F) Bubble plot showing enrichment of the KEGG signaling pathway for genes at the intersection of scRNA-seq and mRNA-seq. t-SNE, t-distributed stochastic neighbor embedding; KEGG, Kyoto Encyclopedia of Genes and Genomes.

HAVCR2, MDK-(ITGA4 + ITGB1), MDK-LRP1, MDK-NCL, MDK-SDC2, THBS1-CD36, and *THBS1-CD47*. The highly expressed ligand-receptor pairs for smooth muscle cells as senders and macrophages as receivers were *ANXA1-FPR1, APP-CD74, CD99-PILRA, COL1A1-CD44, COL1A2-CD44, COL4A1-CD44, COL4A2-CD44,* *COL6A1-CD44, COL6A2-CD44, CXCL12-CXCR4, FN1-(ITGA4 + ITGB1), COL6A3-CD44, FN1-CD44, HLA-DPA1-CD4, HLA-DPB1-CD4, HLA-DRA-CD4, HLA-DRB1-CD4, HLA-F-LILRB1, LAMA4-CD44, LAMB2-CD44, THBS2-CD47,* and *THBS2-CD36*. The highly expressed ligand-receptor pairs for endothelial cells as

Figure 9 Analysis of cellular communication in atherosclerotic endothelial cells, fibroblasts, macrophages, and smooth muscle cells. (A) scRNA-seq and mRNA-seq differential gene PPI analysis between atherosclerotic and non-atherosclerotic plaque groups. (B) Comparison of the number and intensity of cellular communication between atherosclerotic and non-atherosclerotic plaque groups. (C) Conserved and specific signaling pathway analysis between atherosclerotic and non-atherosclerotic plaque groups. (D) Global signaling pathway analysis of atherosclerotic and non-atherosclerotic plaque groups. (E) Bubble plot showing ligand-receptor pairs that are increased in cell-to-cell communication in atherosclerotic plaque groups. (F) Bubble plot ligand-receptor pairs reduced in cell-cell communication in atherosclerotic plaque groups. Blue represents the non-atherosclerotic plaque group and red represents the atherosclerotic plaque group; Norm, non-atherosclerotic plaque group; Athe, atherosclerotic plaque group. PPI, protein-protein interaction.

senders and smooth muscle cells as receivers were *CD99-CD99*, *COL4A1-(ITGA1 + ITGB1)*, *COL4A1-CD44*, *COL4A2-(ITGA1 + ITGB1)*, *COL6A2-(ITGA1 + ITGB1)*, *FN1-(ITGA8 + ITGB1)*, *FN1-(ITGAV + ITGB1)*, *JAM2-(ITGAV + ITGB1)*, *LAMA4-CD44*, *LAMB1-(ITGA1 + ITGB1)*, *LAMB1-CD44*, *POSTN-(ITGAV + ITGB5)*, and *THBS1-CD47* (*Figure 9E*). Additionally, we analyzed the decreased ligand-receptor pairs in atherosclerotic tissue, with endothelial cells as senders and macrophages as receivers, and the results showed thirteen ligand-receptor pairs were decreased, and MIF was the main ligand. Among endothelial cells as senders and smooth muscle cells as recipients, seven ligand-receptor pairs decreased in the plaque group, and the ligand was mainly MDK, while with fibroblasts as senders and macrophages as receivers, 17 ligand-receptor pairs were decreased in the plaque group, and CD44 and CD4 receptors accounted for a larger proportion. With fibroblasts as senders and smooth muscle cells as receivers, 12 ligand-receptor pairs decreased in the plaque group, with ITGA1 + ITGB1 receptors A making up a large proportion (*Figure 9F*).
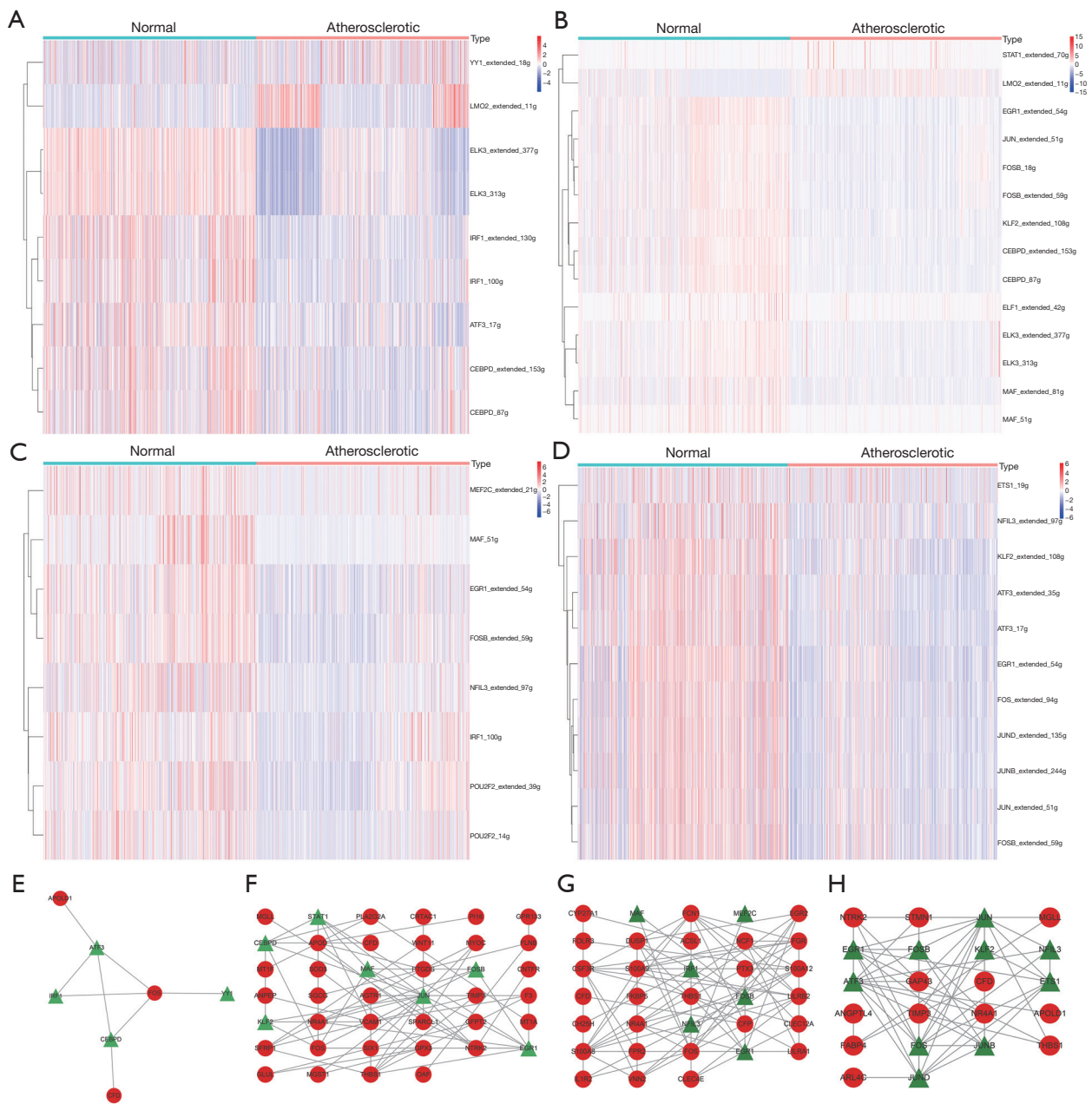
Analysis of cellular transcription factors

We used the "RcisTarget" package in R to identify transcription factors with direct regulatory links in endothelial cells, fibroblasts, macrophages, and smooth muscle cells. Differential analysis of transcription factors was performed in this study. Compared with proximal normal tissue, the plaque group showed low expression of ATF3_17g, IRF1_extended_130g, IRF1_100g, CEBPD_extended_153g, CEBPD_87g, ELK3_extended_377g, and ELK3_313g, and high expression of YY1_extended_18g and LMO2_extended_11g in endothelial cells (*Figure 10A*). JUN_extended_51g, KLF2_extended_108g, FOSB_18g, ELK3_extended_377g, ELK3_313g, FOSB_extended_59g, ELF1_extended_42g, EGR1_extended_54g, CEBPD_extended_153g, CEBPD_87g, MAF_extended_81g, and MAF_51g were less expressed in fibroblasts, while LMO2_extended_11g and STAT1_extended_70g were highly expressed (*Figure 10B*). EGR1_extended_54g, FOSB_extended_59g, POU2F2_extended_39g, POU2F2_14g, IRF1_100g, NFIL3_extended_97g, MAF_51g, and MEF2C_extended_21g were less expressed in macrophages (*Figure 10C*). JUN_extended_51g, ETS1_19g, JUND_extended_135g, JUNB_extended_244g, FOSB_extended_59g, KLF2_extended_108g, NFIL3_extended_97g, FOS_extended_94g, EGR1_extended_54g, ATF3_extended_35g, and ATF3_17g were less expressed in smooth muscle cells (*Figure 10D*). We then constructed a regulatory network of up- and downregulated genes and cell-activated transcription factors in endothelial cells, fibroblasts, macrophages, and smooth muscle cells using scRNA-seq and mRNA-seq. In the regulatory network, endothelial transcription factors were ATF3, IRF1, CEBPD, and YY1 (*Figure 10E*); fibroblast transcription factors were STAT1, CEBPD, MAF, FOSB, JUN, KLF2, and EGR1 (*Figure 10F*); macrophage transcription factors were MAF, MEF2C, IRF1, FOSB, NFIL3, and EGR1 (*Figure 10G*); and transcription factors for smooth muscle cells were JUN, EGR1, FOSB, KLF2, NFIL3, ATF3, ETS1, FOS, JUNB, and JUND (*Figure 10H*).

Discussion

In this study, we generated single-cell profiles of atherosclerotic endothelial cells, fibroblasts, macrophages, and smooth muscle cells via pooled analysis using scRNA-seq of carotid atherosclerotic samples. In addition, by combining aortic atherosclerosis mRNA-seq and metabolome data with scRNA-seq analysis, we revealed the complexity and potential roles of endothelial cells, fibroblasts, macrophages, and smooth muscle cells in the disease.

We found atherosclerotic endothelial cells were mostly of the *ITLN1*, *CCL5*, and *SOST* subtypes, and atherosclerotic smooth muscle cells were mainly of the TFPI2 subtype. The occurrence of atherosclerosis is related to parathyroid hormone synthesis, growth hormone synthesis, secretion, and action, the estrogen signaling pathway, the cGMP-PKG signaling pathway, and chemokine signaling pathways. Comparing endothelial cells between the normal and plaque groups showed the transcription factor YY1 was highly expressed in the plaque group, and ATF3, IRF1, and CEBPD were all expressed at low levels. The transcription factor-target gene network showed FOS regulated YY1, ATF3, IRF1, and CEBPD. FOS is widely expressed in a variety of animal cells, and a study has shown its abnormal expression may contribute to the pathogenesis of hypertension, cardiac hypertrophy, atherosclerosis, and other diseases [22]. C-FOS is a product of the *FOS* gene that contributes to the regulation of inflammatory cytokines, and TNF-α was shown to upregulate IL-6 in VSMCs (vascular smooth muscle cell) via c-FOS [23]. Chlamydia pneumoniae infection was also seen to activate c-FOS in human coronary artery endothelial cells and

Figure 10 Atherosclerotic transcription factor analysis. (A) Differential analysis of transcription factors in endothelial cells in atherosclerotic compared with non-atherosclerotic plaque groups. (B) Differential analysis of transcription factors in fibroblasts in atherosclerotic compared with non-atherosclerotic plaque groups. (C) Differential analysis of transcription factors in macrophages in atherosclerotic compared with non-atherosclerotic plaque groups. (D) Differential analysis of transcription factors in the atherosclerotic plaque group in smooth muscle cells in atherosclerotic compared with non-atherosclerotic plaque groups. Blue represents the non-atherosclerotic plaque group, and red represents the atherosclerotic plaque group. (E) Interaction analysis between transcription factors and differential gene proteins in endothelial cells. (F) Interaction analysis between transcription factors and DEG proteins in fibroblasts. (G) Interaction analysis between transcription factors and differentially expressed genes in macrophages. (H) Interaction analysis between transcription factors and differential gene proteins in smooth muscle cells. Green represents transcription factors and red represents differentially expressed genes. DEG, differentially expressed gene.

accelerated disease progression (24).

Fibroblasts produce extracellular matrix fibers, such as collagen types I and III, proteoglycans, and fibronectin, and are the most common cells in the adventitia of normal blood vessels (25). After activation, myofibroblasts express α-smooth muscle actin, and activated adventitial fibroblasts can promote neointimal and fibrous cap formation. scRNA-seq analysis of mouse aorta showed fibroblasts as the second most common cells after removal of perivascular adipose tissue and that they were plastic and heterogeneous (26-28). We grouped fibroblasts in carotid atherosclerotic tissue into RGS5, APOD (29), SFRP5, and GZMA fibroblast subtypes and reconfirmed their plasticity and heterogeneity. Subsequently, we found APOD fibroblasts gradually differentiated into SFRP5, RGS5, and GZMA fibroblasts during the transition from healthy blood vessels to atherosclerotic ones. These cells were associated with the renin-angiotensin system, the MAPK signaling pathway, the AGE-RAGE signaling pathway in diabetic complications, fluid shear stress and atherosclerosis, drug metabolism (cytochrome P450), metabolism of xenobiotics by cytochrome P450, and other signaling pathways, which has rarely been reported in a previous study (30). Surprisingly, our combined mRNA-seq, scRNA-seq, and untargeted metabolomics analysis of atherosclerosis revealed the AGE-RAGE signaling pathway in diabetic complications has important implications in the atherosclerotic process. Advanced glycation end product (AGE) and receptor for AGE (RAGE) signaling pathways have been shown to contribute to arterial stiffness, atherosclerosis, mitochondrial dysfunction, oxidative stress, calcium homeostasis, and cytoskeletal function, and to regulate the pathogenesis of cardiovascular disease (27). Therefore, the study of AGE-RAGE signaling in fibroblasts should be a priority for atherosclerosis research.

It is well known that phenotypic dysregulation of macrophages is a major driver of atherosclerosis (31). In many diseases, chronic inflammation leads to aberrant remodeling of macrophage responses and changes in their phenotype, leading to an increase in pro-inflammatory macrophages (32). Macrophages have a variety of functional phenotypes in response to specific pathogens, injury-associated molecular patterns, and host-derived signaling molecules (33). The classical model of macrophage polarization describes two opposite phenotypic states: A pro-inflammatory M1 macrophage, induced by bacterial lipopolysaccharide and/or interferon gamma, and an anti-inflammatory M2 macrophage triggered by interleukin

4 (34). However, macrophage phenotypes have been reported to be more than M1 and M2 phenotypes and may be a phenotypic profile combining cytokine and functional features (35,36). In the present study we found macrophage-related differential genes were mostly enriched in osteoclast differentiation, B cell receptor signaling pathways, IL-17 signaling pathways, fluid shear stress and atherosclerosis, primary bile acid biosynthesis, and PPAR signaling pathways. Subsequent subgrouping of macrophages and pseudo-chronological analysis showed that when normal tissues developed into atherosclerotic ones, CCL13 monocytes evolved into C1QB, APOBEC3A, and FABP4 monocytes of the M2 phenotype (37,38). In addition, we found six transcription factors, MAF, MEF2C, IRF1, FOSB, NFIL3, and EGR1, were all reduced in atherosclerotic plaques compared to the surrounding normal vessels, which shows the number and strength of intercellular interactions are weakened when the vessels become atherosclerotic.

We used pseudo-chronological analysis to show atherosclerotic tissues mostly comprise TFPI2 smooth muscle cells, because compared with unaffected arteries, atherosclerosis-related cytokines such as IL-1β and TNF-α act to promote the expression of TFPI2 (39) and act to protect the extracellular matrix produced by smooth muscle cells (40,41). In addition, compared with surrounding normal tissues, smooth muscle cell differential gene signaling pathways were enriched in the MAPK signaling pathway, regulation of lipolysis in adipocytes, the PPAR signaling pathway, IL-17 signaling pathways, and the PI3K-Akt signaling pathway. Several recent studies have shown that smooth muscle cells are an important source of foam cells in atherosclerosis in humans and mice (42,43) and that they promote lipid retention by secreting positively charged apolipoprotein B prior to the presence of monocytes/macrophages in atherosclerotic lesions (44). In addition, during the development of foam cells, macrophages can promote the proliferation of smooth muscle cells (45), which contribute to the adhesion, recruitment, and survival of monocytes. This aggravates the inflammatory response and further promotes the proliferation of smooth muscle cells. Smooth muscle cells can also convert into a macrophage-like phenotype (46). We analyzed cell-cell interaction relationships in atherosclerotic tissues through CellChat and found CD99, APP, JAM, PROS, PERIOSTIN, VCAM, and SPP1 were activated in cells from the plaque group. Receptor-ligand pair analysis of smooth muscle cells (SMCs) and macrophages also showed CD99 and APP were increased in smooth muscle cells. CD99 is a highly

O-glycosylated outer membrane protein (47) which plays a fundamental role in the migration of monocytes across the arterial endothelial cell monolayer, and current research aims to develop anti-atherosclerosis vaccines against it (48). In addition, APP is an evolutionarily conserved protein expressed in cerebral and peripheral arterial endothelial cells (49), and when it is mutated and overexpressed, fatty streak lesions and endothelial dysfunction occur in the aorta (50,51). A animal study has shown the overexpression of mutant APP can accelerate the development of aortic atherosclerosis in ApoE-deficient mice (52) and our study showed CD99 and APP may also play key roles in the interaction between smooth muscle cells and macrophages.

Conclusions

In conclusion, with the wide application of scRNA-seq technology in diseases, over-characterization enrichment (KEGG signaling pathway enrichment, GSVA), GSEA and other methods are used to discover the relationship between pathological signaling pathways and diseases. These lay a theoretical foundation for revealing genetic information such as gene expression networks, heterogeneity, and random expression of immune cells, and provide researchers with disease treatment options. However, scRNA-seq is still time-consuming, costly, and has various unavoidable technical errors (destruction or loss of effective cells, low coverage, sequencing bias, high error rate, limited throughput), and high technical requirements. , and single-cell sequencing tends to be discrete cell types and cell states, which may deviate from true cell-to-cell signaling. We performed a comprehensive bioinformatics analysis of atherosclerotic plaque scRNA-seq, mRNA-seq, and untargeted metabolomics, and in-depth characterization of endothelial cells, fibroblasts, macrophages, and smooth muscle cells. Multi-omics-based comprehensive analysis revealed atherosclerosis-related central genes and key metabolic molecules, cell subsets, cell phenotypic changes in atherosclerotic plaques, intercellular communication patterns, and key transcription factors. These results provide more ideas for determining the mechanism of, and targeting interventions in, atherosclerosis. In future research, the screened central genes, metabolic molecules, important cell subsets, intercellular communication patterns and key transcription factors can be combined with clinical data of patients with atherosclerosis markers, using machine learning, deep learning and other methods, with to explore the diagnosis and prognosis of atherosclerosis, and to find related molecular markers.

This study has two main limitations. First, since we only collected a small number of samples, it is necessary to increase the number of atherosclerotic plaques to verify our findings. Second, due to space limitations, we have only reported epithelial cells, fibroblasts, macrophages, and smooth muscle cells in detail. T cells, B cells, and others have not been studied in depth and will be discussed in future studies.

Acknowledgments

Footnote

Reporting Checklist: The authors have completed the MDAR reporting checklist. Available at https://atm.amegroups.com/article/view/10.21037/atm-22-4852/rc

Data Sharing Statement: Available at https://atm.amegroups.com/article/view/10.21037/atm-22-4852/dss

Conflicts of Interest: All authors have completed the ICMJE uniform disclosure form (available at https://atm.amegroups.com/article/view/10.21037/atm-22-4852/coif). The authors have no conflicts of interest to declare.

Ethical Statement: The authors are accountable for all aspects of the work in ensuring that questions related to the accuracy or integrity of any part of the work are appropriately investigated and resolved. This study was conducted in accordance with the Declaration of Helsinki (as revised in 2013) and was approved by the Medical Ethics Committee of the Second Hospital of Shanxi Medical University (No. 2021YX138). Written informed consent was obtained from all subjects.

Open Access Statement: This is an Open Access article distributed in accordance with the Creative Commons Attribution-NonCommercial-NoDerivs 4.0 International

References

1. Pirillo A, Casula M, Olmastroni E, et al. Global epidemiology of dyslipidaemias. Nat Rev Cardiol 2021;18:689-700.

2. Valanti EK, Dalakoura-Karagkouni K, Siasos G, et al. Advances in biological therapies for dyslipidemias and atherosclerosis. Metabolism 2021;116:154461.

3. World Health Organization. Cardiovascular diseases (CVDs) Fact Sheet. 2021.

4. Gallino A, Aboyans V, Diehm C, et al. Non-coronary atherosclerosis. Eur Heart J 2014;35:1112-9.

5. Ross R. Atherosclerosis--an inflammatory disease. N Engl J Med 1999;340:115-26.

6. Group PR. Relationship of atherosclerosis in young men to serum lipoprotein cholesterol concentrations and smoking. JAMA 1990;264:3018-24.

7. Kayashima Y, Maeda-Smithies N. Atherosclerosis in Different Vascular Locations Unbiasedly Approached with Mouse Genetics. Genes (Basel) 2020;11:1427.

8. Tesić DS. Anatomic distribution of peripheral atherosclerosis and its correlation with lipid disorders. Med Pregl 2009;62 Suppl 3:75-9.

9. Kazum S, Eisen A, Lev EI, et al. Prevalence of Carotid Artery Disease among Ambulatory Patients with Coronary Artery Disease. Isr Med Assoc J 2016;18:100-3.

10. Fernandez DM, Giannarelli C. Immune cell profiling in atherosclerosis: role in research and precision medicine. Nat Rev Cardiol 2022;19:43-58.

11. Yu C, Luo X, Zhan X, et al. Comparative metabolomics reveals the metabolic variations between two endangered Taxus species (T. fuana and T. yunnanensis) in the Himalayas. BMC Plant Biol 2018;18:197.

12. Robinson MD, McCarthy DJ, Smyth GK. edgeR: a Bioconductor package for differential expression analysis of digital gene expression data. Bioinformatics 2010;26:139-40.

13. Li Y, Fang J, Qi X, et al. Combined Analysis of the Fruit Metabolome and Transcriptome Reveals Candidate Genes Involved in Flavonoid Biosynthesis in Actinidia arguta. Int J Mol Sci 2018;19:1471.

14. Hao Y, Hao S, Andersen-Nissen E, et al. Integrated analysis of multimodal single-cell data. Cell 2021;184:3573-3587.e29.

15. Butler A, Hoffman P, Smibert P, et al. Integrating single-cell transcriptomic data across different conditions, technologies, and species. Nat Biotechnol 2018;36:411-20.

16. Aibar S, González-Blas CB, Moerman T, et al. SCENIC: single-cell regulatory network inference and clustering. Nat Methods 2017;14:1083-6.

17. Trapnell C, Cacchiarelli D, Grimsby J, et al. The dynamics and regulators of cell fate decisions are revealed by pseudotemporal ordering of single cells. Nat Biotechnol 2014;32:381-6.

18. Jin S, Guerrero-Juarez CF, Zhang L, et al. Inference and analysis of cell-cell communication using CellChat. Nat Commun 2021;12:1088.

19. Wu T, Hu E, Xu S, et al. clusterProfiler 4.0: A universal enrichment tool for interpreting omics data. Innovation (Camb) 2021;2:100141.

20. Franceschini A, Szklarczyk D, Frankild S, et al. STRING v9.1: protein-protein interaction networks, with increased coverage and integration. Nucleic Acids Res 2013;41:D808-15.

21. Chin CH, Chen SH, Wu HH, et al. cytoHubba: identifying hub objects and sub-networks from complex interactome. BMC Syst Biol 2014;8 Suppl 4:S11.

22. Miao G, Zhao X, Chan SL, et al. Vascular smooth muscle cell c-Fos is critical for foam cell formation and atherosclerosis. Metabolism 2022;132:155213.

23. Zickler D, Luecht C, Willy K, et al. Tumour necrosis factor-alpha in uraemic serum promotes osteoblastic transition and calcification of vascular smooth muscle cells via extracellular signal-regulated kinases and activator protein 1/c-FOS-mediated induction of interleukin 6 expression. Nephrol Dial Transplant 2018;33:574-85.

24. Wang A, Al-Kuhlani M, Johnston SC, et al. Transcription factor complex AP-1 mediates inflammation initiated by Chlamydia pneumoniae infection. Cell Microbiol 2013;15:779-94.

25. Singh S, Torzewski M. Fibroblasts and Their Pathological Functions in the Fibrosis of Aortic Valve Sclerosis and Atherosclerosis. Biomolecules 2019;9:472.

26. Kalluri AS, Vellarikkal SK, Edelman ER, et al. Single-Cell Analysis of the Normal Mouse Aorta Reveals Functionally Distinct Endothelial Cell Populations. Circulation 2019;140:147-63.

27. Lee TW, Kao YH, Chen YJ, et al. Therapeutic potential of vitamin D in AGE/RAGE-related cardiovascular diseases.

Cell Mol Life Sci 2019;76:4103-15.

28. Khan AW, Paneni F, Jandeleit-Dahm KAM. Cell-specific epigenetic changes in atherosclerosis. Clin Sci (Lond) 2021;135:1165-87.

29. Zhang X, van Rooij JGJ, Wakabayashi Y, et al. Genome-wide transcriptome study using deep RNA sequencing for myocardial infarction and coronary artery calcification. BMC Med Genomics 2021;14:45.

30. Shao D, Liu X, Wu J, et al. Identification of the active compounds and functional mechanisms of Jinshui Huanxian formula in pulmonary fibrosis by integrating serum pharmacochemistry with network pharmacology. Phytomedicine 2022;102:154177.

31. Moore KJ, Sheedy FJ, Fisher EA. Macrophages in atherosclerosis: a dynamic balance. Nat Rev Immunol 2013;13:709-21.

32. Schultze JL, Schmieder A, Goerdt S. Macrophage activation in human diseases. Semin Immunol 2015;27:249-56.

33. Ginhoux F, Schultze JL, Murray PJ, et al. New insights into the multidimensional concept of macrophage ontogeny, activation and function. Nat Immunol 2016;17:34-40.

34. Kuznetsova T, Prange KHM, Glass CK, et al. Transcriptional and epigenetic regulation of macrophages in atherosclerosis. Nat Rev Cardiol 2020;17:216-28.

35. Xue J, Schmidt SV, Sander J, et al. Transcriptome-based network analysis reveals a spectrum model of human macrophage activation. Immunity 2014;40:274-88.

36. Colin S, Chinetti-Gbaguidi G, Staels B. Macrophage phenotypes in atherosclerosis. Immunol Rev 2014;262:153-66.

37. O'Rourke SA, Neto NGB, Devilly E, et al. Cholesterol crystals drive metabolic reprogramming and M1 macrophage polarisation in primary human macrophages. Atherosclerosis 2022;352:35-45.

38. Zhao B, Wang D, Liu Y, et al. Six-Gene Signature Associated with Immune Cells in the Progression of Atherosclerosis Discovered by Comprehensive Bioinformatics Analyses. Cardiovasc Ther 2020;2020:1230513.

39. Herman MP, Sukhova GK, Kisiel W, et al. Tissue factor pathway inhibitor-2 is a novel inhibitor of matrix metalloproteinases with implications for atherosclerosis. J Clin Invest 2001;107:1117-26.

40. Libby P. Molecular bases of the acute coronary syndromes. Circulation 1995;91:2844-50.

41. Lafont A, Libby P. The smooth muscle cell: sinner or saint in restenosis and the acute coronary syndromes? J Am Coll Cardiol 1998;32:283-5.

42. Lacolley P, Regnault V, Segers P, et al. Vascular Smooth Muscle Cells and Arterial Stiffening: Relevance in Development, Aging, and Disease. Physiol Rev 2017;97:1555-617.

43. Chistiakov DA, Melnichenko AA, Myasoedova VA, et al. Mechanisms of foam cell formation in atherosclerosis. J Mol Med (Berl) 2017;95:1153-65.

44. Allahverdian S, Chaabane C, Boukais K, et al. Smooth muscle cell fate and plasticity in atherosclerosis. Cardiovasc Res 2018;114:540-50.

45. Wang Y, Dubland JA, Allahverdian S, et al. Smooth Muscle Cells Contribute the Majority of Foam Cells in ApoE (Apolipoprotein E)-Deficient Mouse Atherosclerosis. Arterioscler Thromb Vasc Biol 2019;39:876-87.

46. Beck-Joseph J, Lehoux S. Molecular Interactions Between Vascular Smooth Muscle Cells and Macrophages in Atherosclerosis. Front Cardiovasc Med 2021;8:737934.

47. Muller WA. Leukocyte-endothelial cell interactions in the inflammatory response. Lab Invest 2002;82:521-33.

48. Tourani M, Karkhah A, Najafi A. Development of an epitope-based vaccine inhibiting immune cells rolling and migration against atherosclerosis using in silico approaches. Comput Biol Chem 2017;70:156-63.

49. d'Uscio LV, Das P, Santhanam AV, et al. Activation of PPARδ prevents endothelial dysfunction induced by overexpression of amyloid-β precursor protein. Cardiovasc Res 2012;96:504-12.

50. d'Uscio LV, He T, Katusic ZS. Expression and Processing of Amyloid Precursor Protein in Vascular Endothelium. Physiology (Bethesda) 2017;32:20-32.

51. Li L, Cao D, Garber DW, et al. Association of aortic atherosclerosis with cerebral beta-amyloidosis and learning deficits in a mouse model of Alzheimer's disease. Am J Pathol 2003;163:2155-64.

52. Tibolla G, Norata GD, Meda C, et al. Increased atherosclerosis and vascular inflammation in APP transgenic mice with apolipoprotein E deficiency. Atherosclerosis 2010;210:78-87.